Journal of Marine Systems
May 2023, Volume 240, Pages 103888 (14p.)
https://doi.org/10.1016/j.jmarsys.2023.103888
https://archimer.ifremer.fr/doc/00832/94357/

Sea surface salinity response to variations in the Aleutian Low

Grodsky Semyon A. [1, *], Reul Nicolas [2], Vandemark Douglas [3]

[1] Department of Atmospheric and Oceanic Science, University of Maryland, College Park, MD, USA
[2] Laboratoire d'Océanographie Physique et Spatial (LOPS), Institut Francais pour la Recherche et l'Exploitation de la Mer, Plouzané, France
[3] University of New Hampshire, Durham, NH, USA

* Corresponding author : Semyon A. Grodsky, email address : senya@umd.edu

Abstract :

The strength of the atmospheric Aleutian Low pressure system varies interannually and has a distinct impact on sea surface temperature (SST), sea level, and other oceanic parameters along the North Pacific subarctic front. These impacts are caused by variable zonal winds through their effects on meridional Ekman transport and air-sea fluxes. While the SST response is well known on an interannual (ENSO) to decadal (PDO) scale, the response of sea surface salinity (SSS) is less known due to relatively sparse observations. The SSS response originates in the western Pacific and is concentrated along the North Pacific subarctic front, reaching a few tenths of psu in the upper 100 m, as demonstrated by satellite SSS, Argo salinity data, and model simulations. SSS anomalies, in contrast to SST anomalies, behave like passive tracers that are advected eastward in the North Pacific Current across the whole basin and, unexpectedly, sometimes intensify to the east. After reaching the eastern boundary, they continue predominantly southward along the California coast, remaining detectable by satellite SSS all the way to the southern tip of the California peninsula.

Highlights

► Satellite salinity shows that SSS variability in the North Pacific subarctic front differs from SST variability. ► In contrast to the SST, SSS anomalies (~0.5 psu) propagate eastward crossing the Pacific over five years. ► SSS anomalies continue south along the California coast being detectable until the southern tip of the California peninsula.

Keywords : North pacific, Salinity, Wind, Aleutian low

1. Introduction

The sub-Arctic front (SAF) in the North Pacific forms a boundary between warm, relatively salty subtropical waters and the cooler, fresher water of the sub-Arctic North Pacific (Yuan and Talley, 1996). This frontal region plays an important role in producing upper ocean water masses (Katsura, 2018). As known from sea surface temperature (SST) and sea surface height (SSH) observations, it is perturbed by forcing at a wide range of temporal scales. This range includes periods from monthly-scale westward propagating low mode Rossby Waves (Killworth et al., 1997) to decadal-scale Pacific Decadal Oscillation (PDO, Mantua and Hare, 2002).

The PDO induces a zonal dipole-like SST pattern around the North Pacific SAF. During positive PDO index phases, cold SST anomalies develop in the central and western North Pacific, and warm horseshoe-shaped anomalies in the eastern Pacific boundary (Mantua and Hare, 2002). Similar SST patterns develop at shorter, interannual scales due to El Niño-Southern Oscillation (ENSO)-induced modulations of the atmospheric Aleutian Low through an atmospheric bridge mechanism (Newman et al., 2016). Because PDO- and ENSO-induced SST patterns in the North Pacific are so similar, the PDO is also known as "ENSO-like interdecadal variability" (Zhang et al., 1997). The SST response pattern is mostly standing and contained in the leading Empirical Orthogonal Function (EOF) of anomalous SST in the North Pacific north of 20°N. Other ocean parameters, such as SSH (Cummins et al., 2005), mixed layer depth (Carton et al., 2008), and barrier layer depth (Liu et al., 2009) also exhibit patterns of variability imposed by changes in the Aleutian Low and its associated midlatitude westerly winds, e.g., (Newman et al., 2016). Alternatively, Di Lorenzo et al. (2008) suggest that decadal fluctuations in salinity, nutrients, and fish stocks in the Northeast Pacific are often better correlated with the North Pacific Gyre Oscillation index than with the most widely-used PDO index.

Due to the sparsity of before 2003 salinity data, the corresponding characteristics of salinity variability in the SAF are less studied. Earlier research (Overland et al., 1999) proposes that, while the PDO has an east/west signature in SST, the sea surface salinity (SSS) signature has an NNW/SSE orientation, similar to the pattern of local response to interannual variability in precipitation. In addition to the precipitation-induced local response, both hydrographic sections and Argo data suggest the presence of eastward propagating density-compensating salinity (spiciness) anomalies at thermocline depths (Kouketsu et al., 2017; Sasaki et al., 2010), also

associated with changes in ocean nitrate chemistry (Kouketsu et al., 2020). These density-compensating subsurface salinity anomalies propagate eastward in the North Pacific Current, continue southward along southern California and Baja coasts, enter the Subtropical front between 10°N-20°N, and return to the western Pacific (Sasaki et al., 2010). Based on Argo observations, Wang et al. (2022) found that the spiciness anomalies originate mainly in the outcrop region of the isopycnals, where they are accompanied by the formation/subduction of the mode waters. Normally, they decay downstream along the geostrophic currents. But, some Eastern Subtropical Mode Water spiciness anomalies, in contrast, intensify downstream without a connection to the mixed layer. Furthermore, in the western to central subtropics, the spiciness anomalies may propagate faster than the geostrophic current, indicating additional transport by eddies.

Particular physical mechanisms giving rise to the eastward propagating North Pacific anomalies are a topic of continuing research. In numerical experiments based on a long-term ocean state estimate, Osafune et al. (2020) found that decadal-scale modulations of mixing first induce heat content anomalies in the western boundary region, which move eastward along the boundary between the subtropical and subarctic gyres, taking 10 years to reach the eastern region. Results also suggest that the generation of a spiciness anomaly in the open ocean may play a role. With a focus on the near-surface layer, our analysis of ocean simulations by different models (with special resolution ranging from 0.1 to 0.25°) forced by various observed winds (not shown in this paper) indicates a substantial similarity among eastward propagating SSS anomalies along the North Pacific SAF consistently simulated by these different models. This tentatively suggests that the skill is in the similarity between the observed winds, which variation is the ultimate cause of the eastward SSS anomaly generation.

Due to the subsurface nature of spiciness anomalies, there exists a large degree of uncertainty as to the possibility of their remote sensing detection. Aside from density following subsurface spiciness anomalies, surface-trapped mixed layer salinity anomalies (thus exposed to remote sensing) can also occur. The goal of this paper is to document the presence of such mixed layer salinity anomalies and use the advantage of the panoramic view made available by new sea surface salinity (SSS) satellite data to track the kinematics of these eastward SSS features. These SSS anomalies are advected by local surface currents as quasi-passive tracers, with positive

buoyancy supported by the stably stratified pycnocline beneath the mixed layer. Further evidence of mixed layer salinity anomalies and their advective nature are presented by Ren and Rudnick (2021) from a combination of shipboard hydrography, ocean gliders, and Argo floats. They show that 2017-2019 interannual high-salinity anomalies in the California Current (and anomalously high temperatures) were unique in at least 16-year records, formed earlier in the North Pacific Subtropical Gyre, and then advected into the California Current.

Probably similar eastward propagation of mixed layer salinity anomalies is observed in other basins along eastward geostrophic circulation branches. Such surface-trapped eastward SSS propagation is observed in the equatorial Indian Ocean during negative Indian Ocean dipole events (Sun et al., 2019), with an interruption during El Nino-induced westward current reversals (Grodsky et al., 2001). It is also evident in the Atlantic North Equatorial Countercurrent, which advects eastward salinity anomalies originating in the Amazon plume area (Grodsky et al., 2022).

Here we show that near-surface salinity anomalies associated with interannual and longer changes of midlatitude westerly winds are also present along the North Pacific SAF. Their eastward propagation along the SAF and further southeastward evolution along US west coast is detectable by satellite salinity sensors which can complement the traditional ocean in-situ observations by providing higher temporal and spatial sampling (Reul et al., 2020). The eastward propagation is perhaps most evident when examining SSS, for which advection is important (Foltz et al., 2004), whereas altimeter-detected SSH is dominated by westward planetary waves, and satellite SST signals are attenuated by the negative air-sea heat flux feedback as well as are stronger affected by shorter-scale and more variable air-sea interactions. From a satellite perspective, this emphasizes the potentially beneficial role of SSS in studying the SAF dynamics.

This paper is organized as follows. We begin by analyzing satellite SSS and Argo salinity data to examine the detectability of the eastward propagating near-surface SAF salinity anomalies. A longer-term perspective will also be explored using model simulations. Approaching the west coast, these anomalies follow along a southward pathway in the California Current. This pathway conveys them through the low gradient surface density field of the northeastern Pacific where they impact the mixed layer thermohaline characteristics along the US west coast. The anomalies then sink under less dense water of the Subtropical front. Due to the predominantly

multiyear scale of variability and short time frame of satellite and Argo SSS, intermediate complexity historical GFDL climate model simulations are used to explore the SAF salinity anomaly statistics based on longer model records.

2. Data

In situ data: For upper ocean salinity and temperature, the Scripps Institution of Oceanography (SIO) Argo profile analysis is used. By decomposing data into time mean and monthly mean anomaly fields, this analysis can resolve finer spatial scales for monthly analysis on a global 1°x1° grid from January 2004-ongoing (Roemmich and Gilson, 2009). As a proxy for SSS, the shallowest level of the SIO salinity analysis (2.5m) is used.

Satellite data: Satellite SSH data are obtained from the AVISO multi-satellite merged altimeter dataset, now distributed through the Copernicus Marine Environment Monitoring Service (http://marine.copernicus.eu). Satellite SST data are taken from NOAA Optimally Interpolated (OI) SST V2.1 available since 1980 on a 0.25° grid (Reynolds et al., 2007). Newly available spatially-resolving monthly satellite SSS is explored using the multi-mission Optimally Interpolated Sea Surface Salinity (OISSS) Level 4 V2.0 dataset (https://www.esr.org/data-products/oisss/) available from August 2011 to the present on a 0.25° grid (Melnichenko et al., 2016). This product merges AQUARIUS/SAC-D (August 2011 to June 2015, Kao et al., 2018) and Soil Moisture Active Passive (SMAP) data (April 2015 – present, Meissner et al., 2019), with minor use of Soil Moisture and Ocean Salinity (SMOS) data (Reul et al., 2020). In this product, the two-month overlap between Aquarius and SMAP was used to ensure consistency and continuity in the data record. SMOS data are used only to fill the SMAP data gaps during June – July 2019 and Aug. – Sep. 2022.

Atmospheric reanalysis and model data: The Aleutian Low is characterized using monthly ERA5 reanalysis atmospheric fields that are produced by the European Centre for Medium-Range Weather Forecasts and available from (https://www.ecmwf.int/en/forecasts/datasets/reanalysis-datasets/era5) (Hersbach et al., 2020). Coupled model simulations are used as supplementary data to confirm observation-based findings. For this, we rely on the NOAA/GFDL Earth System Model Version 4.1 (ESM4.1) that is available from the Coupled Model Intercomparison Project (CMIP) version 6 collection of model runs (https://esgf-node.llnl.gov/search/cmip6/) (Dunne et al., 2020). It features intermediate scale horizontal resolution of both atmosphere (2° to 1°) and

ocean (1° to 0.5°). We use 165-year-long historical simulations ('esm-hist' in CMIP6 nomenclature) to explore statistical relationships among SSS, SST, and atmospheric pressure over the North Pacific.

3. Results

3.1 Detectability

We will begin with an examination of the feasibility of the detection of subarctic front salinity anomalies in satellite SSS. Both in-situ Argo (Roemmich and Gilson, 2009) and satellite salinity data show a zonal band of enhanced standard deviation (STD) of monthly SSS anomalies (SSSA, defined as a deviation from the monthly seasonal cycle) along the SAF and extending southeastward approaching the eastern Pacific boundary (Fig. 1). In this paper, the monthly seasonal cycle is defined as the record-long mean for each calendar month, e.g., 2004-present mean for the Argo dataset. As expected, the spatial configuration of the North Pacific enhanced SSS variability area is connected to the mean position of the SAF, in turn suggesting that meridional undulations of this front position produce the observed SSS variability. The characteristic STD magnitude of anomalous SSS in this meridional band (~38° to 46°N) exceeds 0.2 psu making these signals detectable by satellite SSS, e.g., (Meissner et al., 2019). This is confirmed by the similarity of SSS variability patterns derived from satellite (Fig.1a) and in-situ (Fig. 1b) data. Noticeably, the magnitude of SSS variability along the SAF is significant even in comparison with the tropics where it is expectedly stronger, but only by a factor of two.

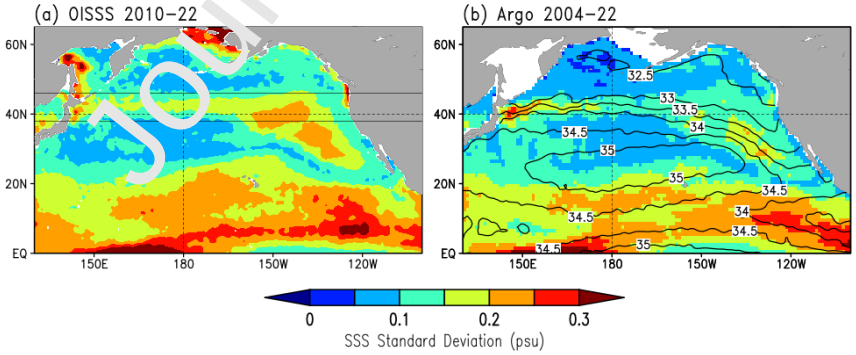

Figure 1. STD deviation of monthly SSS anomalies from (a) optimally interpolated satellite SSS (OISSS) and (b) Argo SIO analysis. Contours are time mean Argo SSS. Two solid lines in (a) bound 38°N-46°N band of higher SSS variability along the North Pacific Subarctic front.

Approaching the US west coast (~150°W–120°W), the North Pacific SSS variability pattern intensifies and shifts southward following the mean SAF configuration (Fig. 1). Due to their presence in the mixed layer, with related mixing and exposure to air-sea heat exchanges, these

SAF SSS anomalies and their west coast extension are not purely spiciness anomalies and can remain at the surface in low gradient density fields. The mixed layer is bottomed by a stably stratified vertical layer (pycnocline). Its positive stability allows for a wide range of mixed layer disturbances that don't overturn the water column. Anomaly sinking develops only when they are advected towards a front with less dense surface waters.

In this paper, we illustrate that interannual near-surface salinity anomalies along southern California and Baja coasts may be related to upstream SAF anomalies and, thus, predictable at multi-year lags. The presence of a low surface density gradient area in the North Pacific eastern boundary (not shown) helps to maintain their surface appearance and enables SSS measurements by remote sensing poleward of the subtropical front latitudes, ~20°N. We expect that these SSS anomalies sink below less dense subtropical front waters, but stay at the surface in the California Current System. Interestingly, the North Pacific SSS variability pattern is likely separated from the pattern of tropical SSS variability (Fig. 1) suggesting that eastward SSS anomalies originating in the SAF don't extend south of the subtropical front and are probably subducted below its less dense waters.

3.2 Eastward propagation

The primary mode of North Pacific subarctic front SST variability is associated with wind-induced meridional shifts that constitute an essential part of PDO variability. But, its SSS variability differs. In contrast to PDO-like quasi-standing SST perturbations (cold/warm SST anomalies in the central and western North Pacific and warm/cold horseshoe-shaped SST anomalies in the eastern North Pacific, e.g., Mantua and Hare, 2002) and ocean planetary wave westward propagation, the SSS shows eastward-propagating (up to ~0.5 psu) anomalies near 40°N that cross the North Pacific, transiting 140-240°E over a few years (Fig. 2).

During the satellite SSS period since 2011, a sequence of three different sign salinity anomalies, (A), (B), and (C), was observed in the SAF region (Fig. 2). The first salty anomaly (A) started developing in the western North Pacific in 2012 (Fig. 2, left, lower red dash line). In 2017-2019, the final stage of its evolution along the US west coast was observed in in-situ data by Ren and Rudnick (2021), who found that the magnitude of this interannual high-salinity anomaly was unique in at least 16-year records in the California Current system.

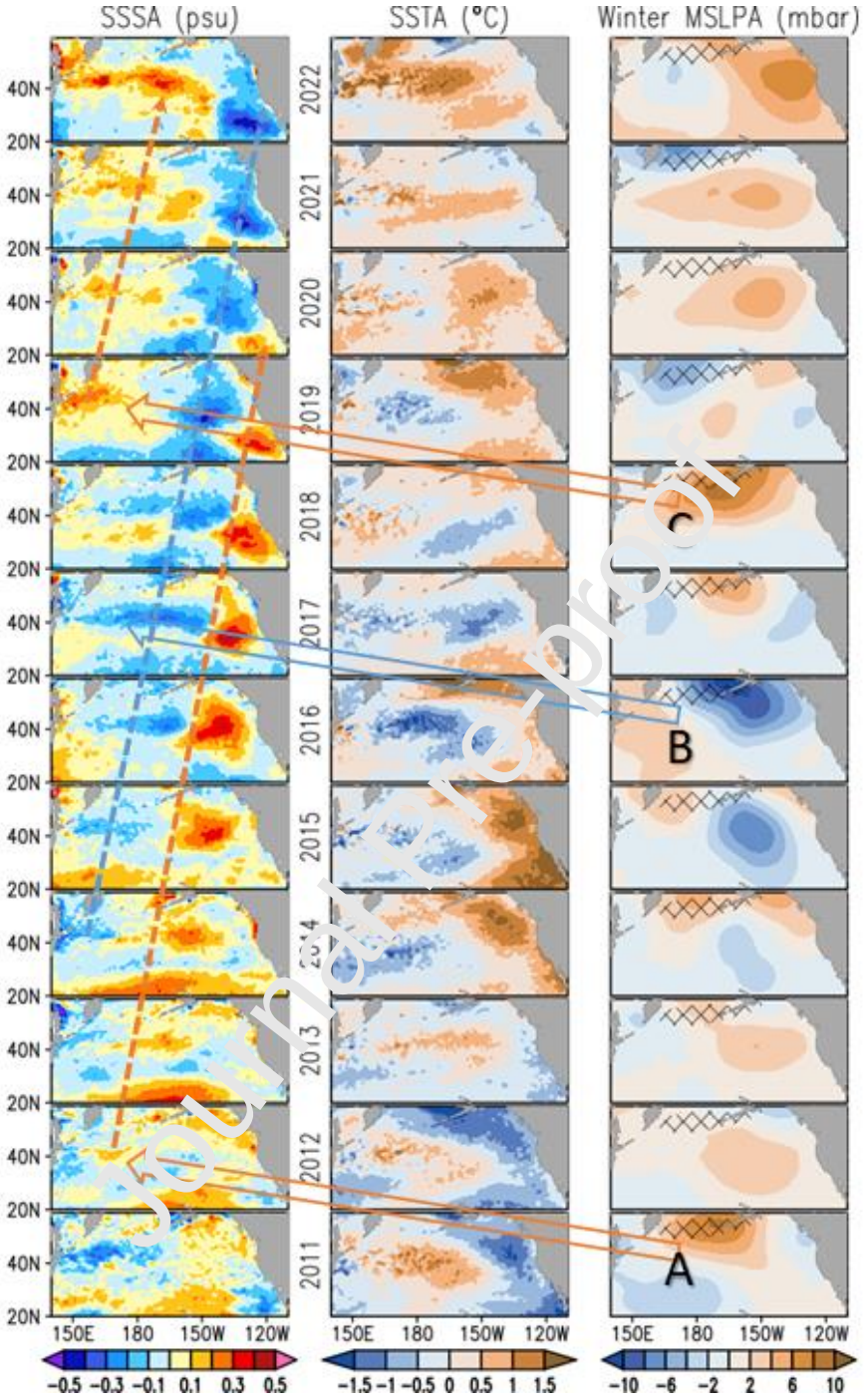

Figure 2. Annual anomalies of satellite SSS (OISSS), SST (NOAA OI SST v2.1), and winter (Nov.-Mar.) anomaly of ERA5 MSLP during satellite SSS period 2011-onward. SSS and SST anomalies are averaged over a calendar year, winter MSLP anomalies are averaged over five months from the previous year Nov. to the current year Mar. The three largest Aleutian Low positive (A, C) and negative (B) MSLP anomalies correspond to salty and fresh SSS anomalies in the western north Pacific, respectively. These salinity anomalies are advected eastward across the entire North Pacific and then southward along the California coast (dashed lines in the left column). The core of winter climatological Aleutian Low (<1003 mbar) is cross-hatched.

This first salty anomaly was followed by a fresh anomaly (B) that started developing in the west in 2014 (Fig. 2, left, blue dash line). This fresh anomaly entered the eastern Pacific boundary in about 2019 and still evolve there propagating southward as of 2022. The latest salty anomaly (C) was first detected in the west in 2019 (Fig. 2, left, top red dash line). As of 2022, it is still propagating eastward across the central north Pacific. The three North Pacific SSS anomalies initiate in the western North Pacific and propagate eastward for around 4 to 5 years before reaching the eastern boundary. They then proceed southward along the coast of California and Baja California and gradually attenuate approaching the southernmost point of the California peninsula near 20°N. Only (A) shows a termination while (B) and (C) are not over yet.

The occurrence of each SSS anomaly may be related to an Aleutian Low anomaly and a PDO-like pattern of anomalous SST. During the 2011-22 period (Fig. 2), a total of three Aleutian Low anomalies spatially coincident with the mean position of the pressure system were observed. The salty anomaly (A) is presumably associated with the reduced Aleutian Low in 2011 (positive MSLP anomaly A in Fig.2) and linked to below-average mid-latitude geostrophic westerly winds (e.g., Newman et al., 2016). Its related anomalous geostrophic easterly winds caused an anomalous northward Ekman advection, which produced salty and warm anomaly in the west by acting on the mean meridional salinity and temperature gradients (Fig. 2). The positive SSTA pattern present in 2011 and 2012 shifted to the east and decayed in 2013. Then it majorly disappears in 2014 (Fig.2, middle column). But, the corresponding SSS anomaly does not. Instead, it is advected eastward by the North Pacific Current and even intensifies as it approaches the eastern boundary in 2015-17 (Fig. 2, left). During 2018-20, the salty anomaly (A) propagates southward and gradually attenuates along the coast (see lower dashed red line in Fig. 2 SSSA panel).

Compared to the salty anomaly (A), the development of a fresh anomaly (B) seems to be more complex. It is first seen in the west in 2014 coincident with cold SST anomaly there (see 2014–16 SSSA and SSTA panels in Fig. 2). But, fresh SSS and cold SST anomalies in the western SAF don't seem to be generated by an anomaly of the Aleutian Low, which amplified only two years later in 2016 (see B in Fig. 2). It can be speculated that Aleutian Low amplification in 2016 may have strengthened already existing fresh SSS anomaly (B) through the anomalous southward Ekman advection while its origination may be related to intrinsic ocean dynamics in

the Kuroshio-Oyashio Extension (KOE) region. Like salty anomaly (A), a salty anomaly (C) is associated with the preceding Aleutian Low attenuation (see C in Fig. 2).

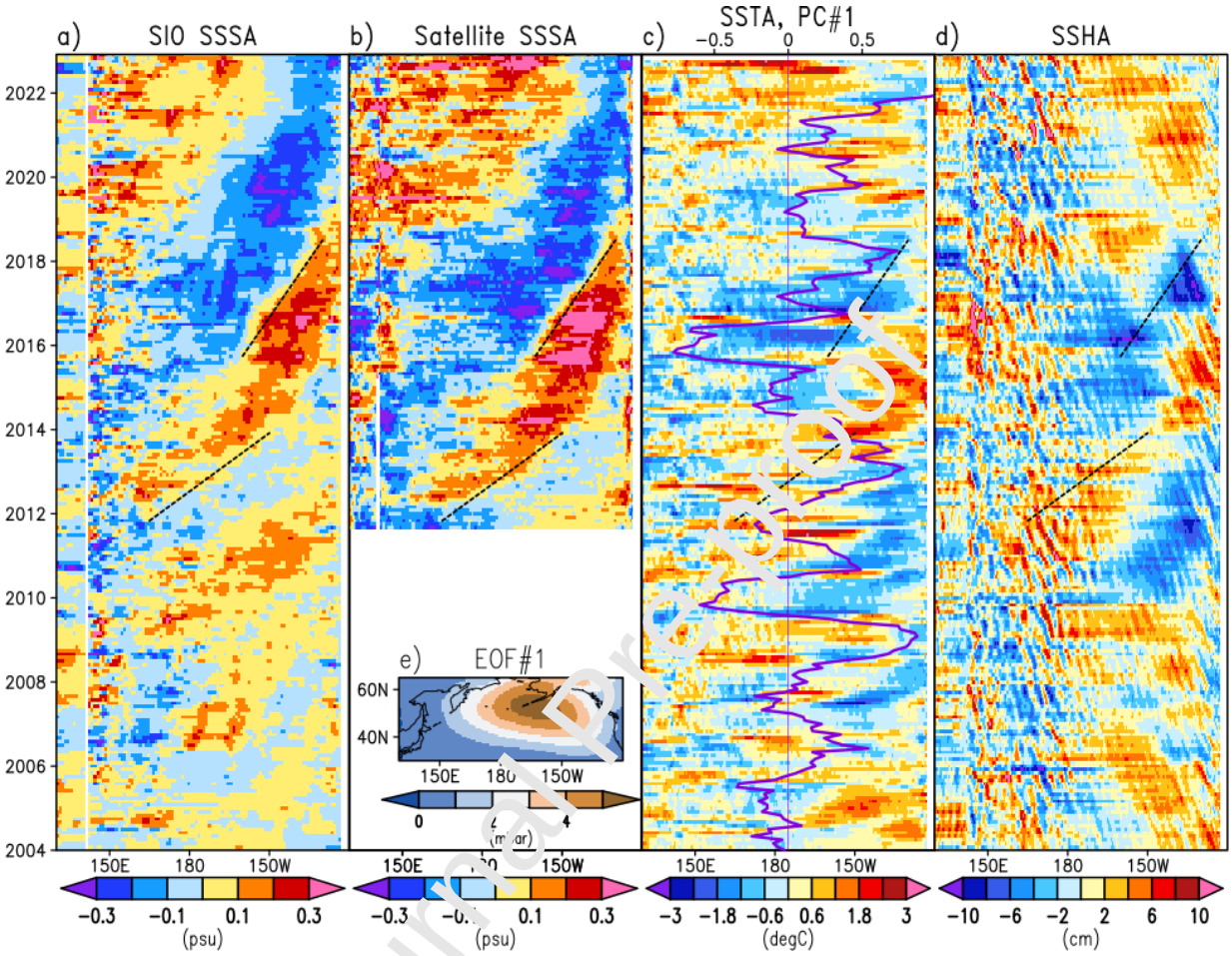

Figure 3. Time-longitude monthly (a) SIO Argo analysis sea surface salinity anomalies (SSSA), (b) satellite SSSA, (c) sea surface temperature anomalies (SSTA), and (d) sea surface height anomalies (SSHA) averaged 38°-40°N. All panels show the same 6 and 3 cm/s slope lines. Running annual mean time series (PC#1) of the leading EOF of ERA5 monthly mean sea level atmospheric pressure anomalies (e) is shown in (c) as the dark purple line.

While Ekman pumping leads to thermocline heaving and generates barotropic mode Rossby waves that propagate westward, density-compensated (spiciness) T– and S–anomalies are produced by wind-induced meridional front displacements. As passive tracers, spiciness anomalies are advected eastward with the mean flow as suggested by (Taguchi and Schneider, 2014) in their analysis of the eastward-propagating heat content anomalies. These subsurface anomalies follow density surfaces and gradually dissipate as they propagate away from the generation site. However, near-surface observations, including satellite SSS, point to several significant deviations from the above scenario. Firstly, the observations in Figs. 3a,b suggest that

eastward salinity anomalies amplify, rather than dissipate as they propagate eastward. This amplification is captured in the Argo shallowest salinity observations as well as satellite SSS. It may be caused by the eastward weakening of the North Pacific Current (hence zonal velocity convergence) which speed decreases from ~6 cm s^{-1} at 180°W to ~ 3 cm s^{-1} east of 140°W (Fig. 3). For surface trapped anomalies, zonal convergence may lead to anomaly growth if it is balanced by vertical rather than meridional divergence (Kouketsu et al., 2017). The observed SSS variability differs substantially from SST and SSH variability (Figs. 3c, d). While SSS variability is dominated by eastward propagating features, temperature, and sea-level signals also show (especially SSH) signatures of westward propagating Rossby waves, with less evidence of eastward propagation.

The magnitude of SAF salinity varies over time. During the SIO Argo analysis period (2004–present), it was greater in recent years compared to a smaller SSSA magnitude before 2009 (Figs. 3a). It should be noted that weaker Argo-observed salinity anomaly magnitude during the initial period of the Argo analysis (2004-06) may reflect by the growth of Argo population during that period. But since then, the Argo data coverage has been relatively homogeneous in time. The recent salinity anomaly intensification corresponds to the period of stronger variability of the Aleutian Low (Fig. 3e, see EOF amplitude, PC, in Fig. 3c), while the period of smaller SSSA magnitudes before 2009 corresponds to a quiet Aleutian Low period before 2008. Independently, analysis of satellite data in (Nakamura, 2003) indicates that the North Pacific-SAF tends to be narrower, with stronger cross-frontal gradients, and shifts northward during weakened surface westerly winds of negative PDO. This may suggest that decadal changes in the SAF cross-frontal structure may also cause changes in the magnitude of the eastward salinity anomalies, and thus govern their long-term variability.

Eastward propagating disturbances dominate the mixed layer salinity variability along the SAF, according to both in-situ and satellite salinity data. Argo data indicate that these salinity anomalies concentrate within the upper ~150 m column. For most of these salinity anomalies, the SSS is, indeed, a good indicator of their magnitude (Fig. 4a). Although all SAF salinity anomalies have their corresponding surface expression, some of them maximize at below 100 m depths. An example of such subsurface salinity anomaly is a fresh anomaly D observed by Argo at ~150 m depth in 2012–15. This anomaly D entered the eastern boundary in 2015 (see longitudes east of 140°W in Fig. 4a, 2015 panel). The surfacing of this fresh anomaly (D) may

explain the 2015–2016 freshening in the Southern California Current observed in satellite SSS (Vazquez-Cuervo and Gomez-Valdes, 2018). In contrast to this earlier subsurface fresh anomaly D (observed during 2012-15 east of 160°W), a succession of two following salty (A, 2013–19, east of 180°W) and fresh (B, 2014–onward, east of 150°E) anomalies (Fig. 4a) both have apparent surface expressions and as is are evident in satellite SSS (Figs. 2-left, 3b).

Four salinity anomalies are visible in the 2004-22 Argo records, presumably emerging after 2009 from the KOE region (west of 150°E, Fig. 4a). The three of them (D, A, and B) are specified in the above paragraph. Anomalies (A, B, and C) are also captured by satellite SSS data (Fig. 2). The latest salty anomaly C developed in 2018-19 west of ~160°E and currently propagates eastward across the North Pacific. At least two salty anomalies (A and B) seen in satellite data (Fig. 2) and Argo vertical sections during 2013–19 and 2014–onward (Fig. 4a) become stronger over time and may thus have a greater impact on the thermohaline properties of the eastern boundary. The intensification of the eastward salinity anomaly is a clear and consistent signal (Fig. 4a). In contrast, the corresponding temperature anomalies (Fig. 4b) do not show any consistent eastward amplification/propagation and do not always accompany salinity anomalies, which is expected given their greater exposure to and weakening due to local air-sea interactions. The tracing of the largest salinity anomalies (A and B), in particular, shows that they are not phased in with their corresponding temperature anomalies (see slope lines in Fig. 4). As a result, these salinity and temperature anomalies are not fully density compensating.

Although Figs. 2 and 3 suggest that midlatitude westerly wind strength modulation associated with Aleutian Low modulation (and its related anomalous SST patterns) is a plausible cause of the eastward salinity anomalies, Fig. 4a shows that the fresh anomaly (B) was only amplified by Aleutian Low strengthening in 2016 (Fig. 2). In fact, it was preceded by fresh anomalies emerging from the KOE region in 2013–14 and present in 2015 (Fig. 4a). This implies the possibility of a superposition between ocean inherent salinity anomalies caused by KOE dynamics and those caused by winds (Nonaka et al., 2020).

Given the limited number of SAF salinity anomaly events observed during Argo and satellite SSS periods, historical climate simulations are explored next to better evaluate the statistical characteristics of these salinity anomalies.

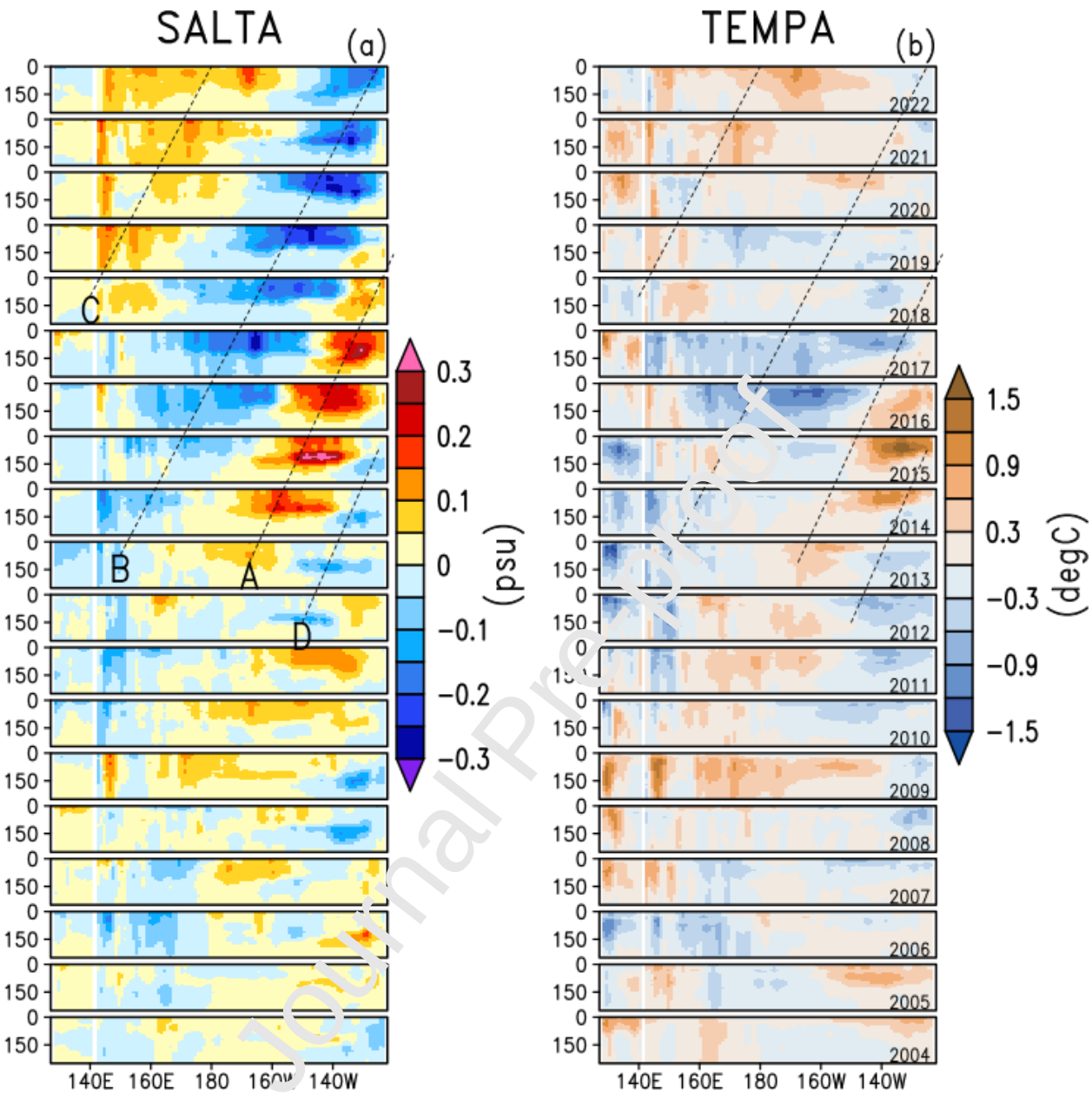

Figure 4. Annual depth-longitude (a) salinity, SALTA, and (b) detrended temperature, TEMPA, anomalies averaged 38°-46°N along the subarctic front. Slope dashed lines (~ 3 cm s^{-1}) follow eastward salinity features (A, B, and C) discussed in Fig.2 based on satellite SSS data. Also, subsurface fresh salinity anomaly (D) is outlined. Data are from the SIO Argo analysis. The same slope lines are shown in panels (a) and (b).

3.3 Model-based analysis

Salinity anomalies in the North Pacific SAF vary in a wide range of time scales including ENSO and PDO periods. Given this multiyear and longer variability, investigating the governing physics of SAF salinity anomalies necessitates decadal or longer model simulations because the

existing high-sampled observations are still too short (Argo-only salinity is available since the early 2000s). They are investigated below using intermediate complexity 165-year-long historical GFDL earth system model simulations. These model data are sufficient to construct meaningful statistics, and reasonably display the mean SAF location and its enhanced SSS variability. In this paper, we investigate the relatively long duration of these simulations to establish statistically significant relationships between S– and T–anomalies with Aleutian pressure low anomalies (which drive regional midlatitude westerly winds).

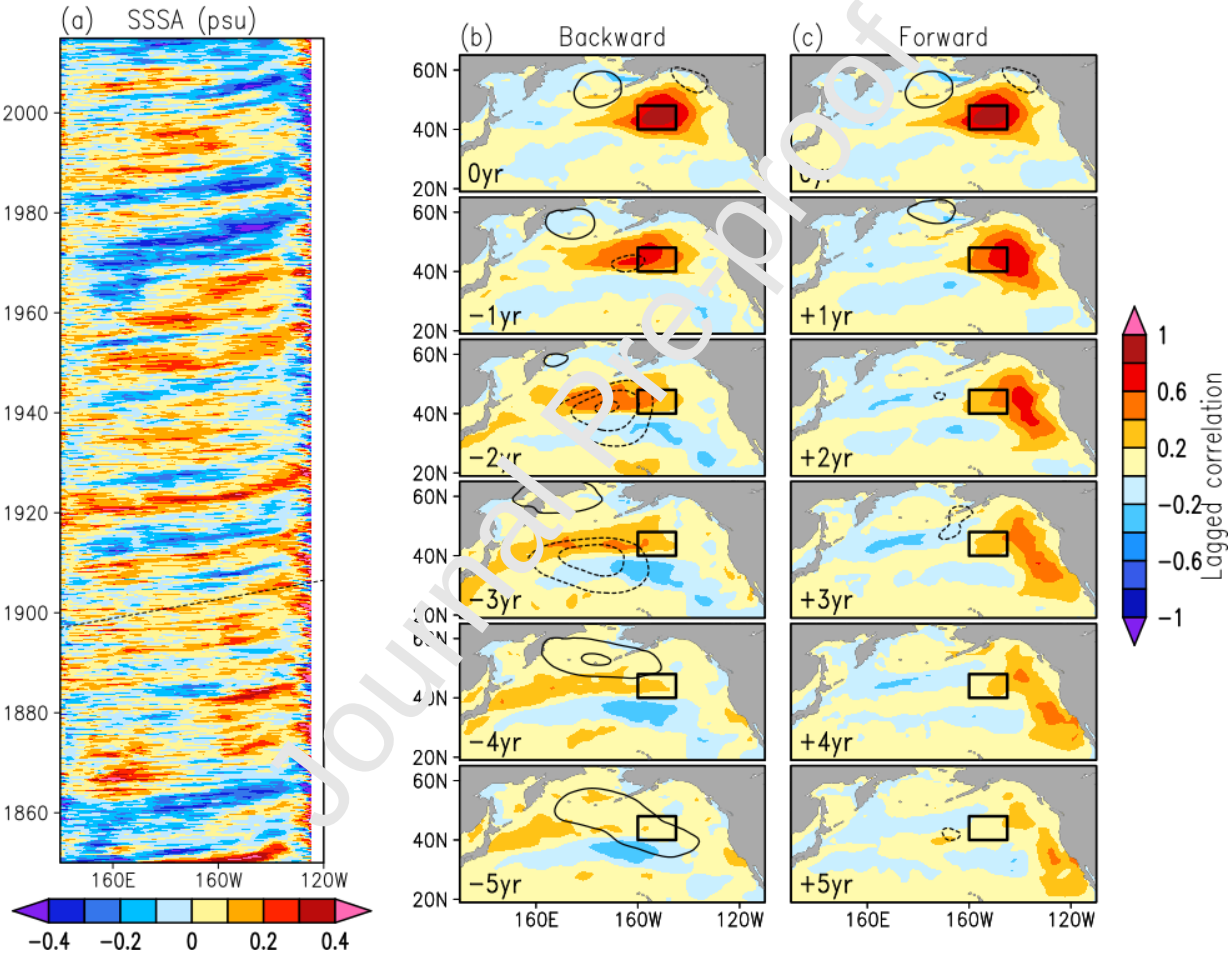

Figure 5. (a) Eastward SSS anomalies (SSSA) along the north Pacific subarctic front (40-48°N) in GFDL ESM4 historical run. The slope line corresponds to 3 cm s^{-1}. (b, c) Lagged correlation of box-averaged (200-215E,40°-48°N) SSSA time series with SSSA elsewhere. Lags are in years. Negative/positive lags correspond to backward/forward evolution relative to the box, respectively. The box is chosen right in the middle of salinity anomaly evolution path to better depict previous (cross Pacific) and forthcoming (along coast) evolution of SSSA patterns. For 165-long model timeseries and interannual periods of SSSA, correlation magnitudes >0.2 are statistically significant at the 99% level. Contours show lagged regressed mean sea level atmospheric pressure anomalies corresponding to 1 psu SSSA in the box. Contours are drawn at [-4 -3 -2 2 3 4] mbar, with positive and negative contours shown by solid and

dash, respectively.

The time-longitude diagram of simulated salinity (Fig. 5a) depicts the presence of 0.3 psu eastward propagating SSSA with an average speed of 3 cm/s, which tends to slow down as it approaches the west coast of the United States. These eastward propagating SSS anomalies are not subducted or attenuated as they propagate to the east along the SAF. Instead, they remain at the surface and some of them even intensify towards the east. Some decadal variations in the strength and polarity of simulated SSS anomalies (with relatively weaker SSSA during 1920-40 followed by stronger SSSA during 1950-90 model years, Fig.5a) may be noticed, as in observations (Figs. 3, 4).

To track the major pathway of SSS anomalies, their time-lagged correlation patterns are built with respect to SSSA time series spatially averaged over an eastern North Pacific box (Figs. 5b, c). By using this eastern box as a reference location (roughly located in the middle of the eastward anomaly life cycle), the preceding (backward) and succeeding (forward) salinity anomaly evolution can be better visualized in correlation patterns. According to this model, SSS anomalies first appear in the KOE region 5 years before passing through the eastern North Pacific box (Fig. 5b). They are advected across the Pacific by the Kuroshio Extension and North Pacific Current for about 5 years after they emerge from the KOE region. By time +1 year, they reach the California/Alaska Current bifurcation in the eastern boundary, from which they continue along a southward pathway, mostly following the California Current (Fig. 5c). In this model, there is little, if any, salinity anomaly propagation along a northern pathway in the Alaska Current. Over the next 5 years following the box passage, the SSS anomalies originated in the SAF are advected in the highly variable California Current System before subducting beneath less dense water of the subtropical front at ~ 20°N. In line with observations (Fig. 2), Fig. 5 depicts an advective evolution of SAF salinity anomalies with a typical lifecycle of about 10 years. The advective behavior of SAF salinity anomalies implies a multi-year time lag between their central North Pacific crossing and west coast appearance, which provides an advective mechanism for such coastal salinity anomalies' predictability. The typical advective lag of about 5 years is expected to define the temporal scale of predictability.

Fig. 5 also presents the lagged regression patterns illustrating expected MSLP anomalies corresponding to 1 psu SSSA in the eastern North Pacific box. One may expect a weakened

Aleutian Low (positive MSLP anomalies there) during the onset of a salty anomaly in the west (larger negative lags in Fig. 5b). Roughly, positive MSLP anomalies are present in the regressed patterns at negative lags, with the most pronounced pattern at lag=–4yr. MSLP regression patterns at lag=–2 and –3 yr also suggest that the effect of positive MSLP anomalies over the Aleutian Low may be augmented by negative MSLP anomalies to the south. But overall, the MSLP regression patterns in Fig. 5 may be not optimal because they are referenced to salinity variability in the eastern North Pacific box, which lags the driving MSLP anomaly by about 5 years.

To better illustrate a relationship between SAF salinity anomalies with the Aleutian pressure low, SSS anomalies are composited for relatively strong positive and negative atmospheric pressure events (Fig. 6). The amplitude of the leading EOF of model atmospheric pressure anomalies, PC, is used to select these events. For a given lag, Δt, composites in Fig. 6 are calculated for positive and negative PC values exceeding 1.5*STD of the leading EOF amplitude:

$$\Delta\mathrm{SSS}^{+} = \overline{H(\mathrm{PC} - 1.5\sigma) \cdot S'(t + \Delta t)} \quad \text{for PC} > 0 \text{ (positive)}$$

$$\Delta\mathrm{SSS}^{-} = \overline{H(-\mathrm{PC} - 1.5\sigma) \cdot S'(t + \Delta t)} \quad \text{for PC} < 0 \text{ (negative)}, \qquad (1)$$

where $H(x > 0) = 1$, $H(x \leq 0) = 0$, S' – SSSA, overbar is the time mean, and σ is the standard deviation of PC.

The positive (left) and negative (right) column in Fig. 6 corresponds to the weakening and strengthening of the Aleutian Low, respectively, with corresponding changes in the strength of midlatitude westerly winds over the North Pacific. The ΔSSS^{+} composite (corresponding to a weakened Aleutian Low and decreased westerly winds) appears complex, with SSS signals of both signs included. This is explained by a periodicity in the appearance of salty and fresh eastward salinity anomalies, with the preceding fresh anomaly, traced by the dashed open arrow in Fig. 6 (positive), which also contributes to the ΔSSS^{+} composite.

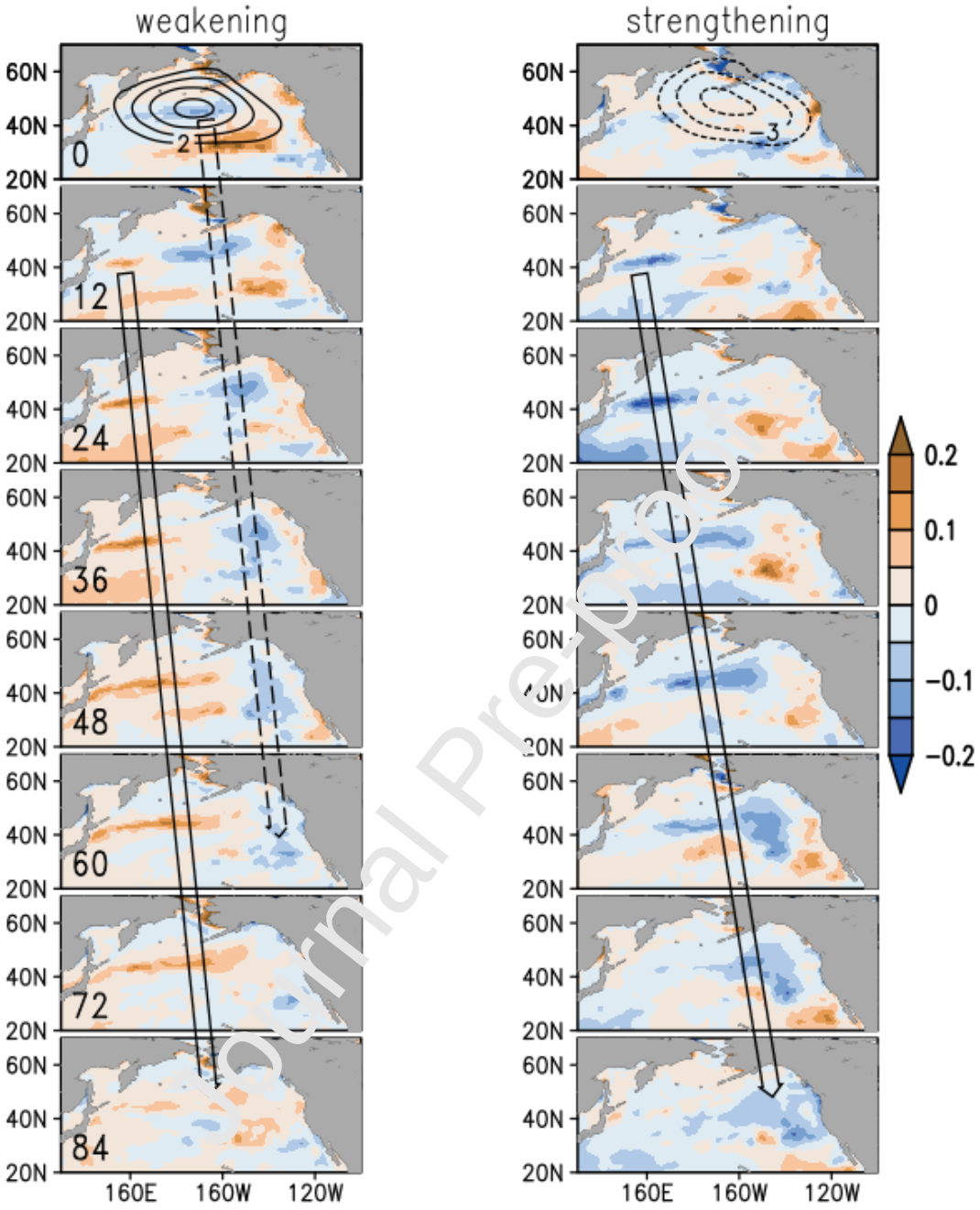

Figure 6. SSS anomaly composites [psu] following (left) weakened and (right) strengthened Aleutian Low with variations exceeding 1.5*STD of the amplitude of the leading EOF of MSLP anomaly computed using Eq. (1). Numbers in left-bottom corners of left column panels are lags (in month) behind MSLP. Open arrows illustrate SSS anomaly propagation. Data are from NOAA/GFDL ESM4 coupled model 165-year historical simulations. Top panels also include MSLP anomaly composites (contour interval 1 mbar, only values >=2 mbar are shown).

Aside from that artifact, the composites show a consistent response of ocean salinity to changes in zonal wind caused by changes in the strength of the Aleutian Low. Even though the ΔSSS^{+} and ΔSSS^{-} composites are derived from nonintersecting data, they confirm that the Aleutian Low

weakening/strengthening produces salty/fresh anomalies, respectively (Fig. 6). In a year or two after a positive MSLP event, a salty anomaly forms in the west. Arguably, it is formed in response to the westerly wind weakening and associated anomalous northward Ekman advection (Fig. 6, left). But, examining potential physical mechanisms governing these salinity anomalies is beyond the scope of this paper. The generated salinity anomaly expands and moves eastward, remaining 'visible' until Lag=72 months. Negative MSLP events (Fig. 6, right), on the other hand, cause fresh anomalies in the west that also propagate eastward. The directions of anomalous winds and anomalous meridional Ekman transport are all consistent with the sign of SSS anomaly, with salty and fresh SSS anomalies originating in response to anomalously weak and strong westerly winds, respectively.

Given this consistent response, a trivariate EOF analysis of concurrent MSLP and SST anomalies, along with 2-year lagged SSSA, is performed.

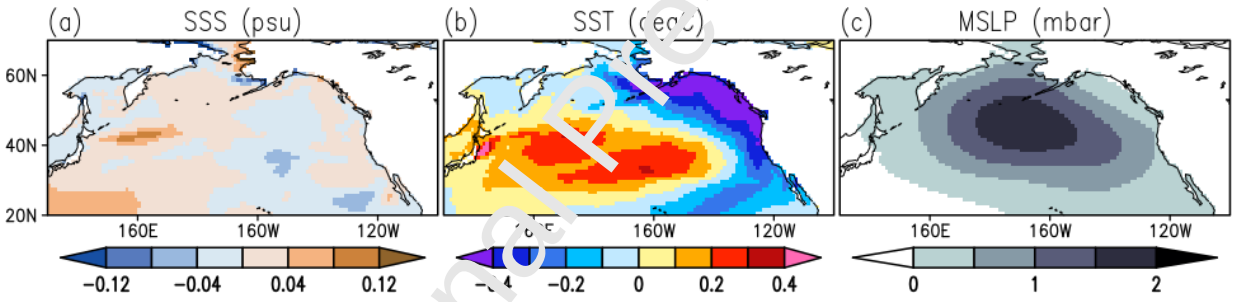

Figure 7. Spatial patterns of the leading trivariate EOF of monthly anomalous (a) SSS, (b) SST, and (c) mean sea level atmospheric pressure (MSLP). Given the delayed response of SSS, concurrent annually smoothed MSLP and detrended SST anomalies are used along with 2-year lagged SSS anomalies. Magnitudes correspond to one standard deviation of the temporal EOF amplitude. Data are from NOAA/GFDL ESM4 ('esm-hist') 165-year historical run.

The leading EOF of anomalous atmospheric mean sea level pressure (Fig. 7c) looks similar to that based on ERA5 atmospheric reanalysis data (Fig. 3e). The EOF analysis in Fig. 7 confirms a close relationship between the Aleutian low variability (Fig. 7c), the development of a typical PDO-like SST response (Fig. 7b), and the origin of a salinity anomaly in the KOE region (Fig. 7a). This correspondence between MSLP and SST patterns has previously been widely discussed, for example (Newman et al., 2016). The SSS pattern is a novel addition to such analyses. Although the SSSA pattern is local and weak, observations such as those in Fig. 2 suggest that it is only the beginning of its evolution. It will evolve over the next 10 years,

crossing the Pacific and progressing southward along the eastern ocean boundary in the California Current.

4. Summary and Discussions

At around 40°N, the sub-Arctic front (SAF) in the North Pacific separates the subtropical gyre from the subpolar gyre. It is detectable in satellite SSS due to a persistent, mostly meridional salinity gradient. Wind-induced meridional shifts in the SAF cause PDO-like standing SST disturbances, and these are the primary signature of SST variability. The SAF is also influenced by westward propagating Rossby waves, which are visible in SSH and, to a lesser extent, in SST.

However, SSS variability in the SAF is noticeably different. In contrast to PDO-like SST perturbations and westward planetary waves, the SSS shows eastward propagating ~0.5 psu anomalies that cross the North Pacific, transiting 140-240°E over a few years. They can be seen in satellite SSS data as well as in-situ ocean data. Vertically-resolved Argo data show that these eastward salinity anomalies occupy the upper 150 m of the water column, indicating that the SSS can be used as a good indicator of their presence. A GFDL Earth System Model 4.1 is also shown to do a good job of simulating these slow multiyear eastward propagating salinity anomalies.

The observed SSS anomalies could be related to density-compensating (warm/salty or cool/fresh) subsurface spiciness anomalies caused by meridional shifts in the SAF interface. The pathway taken by the largest observed salinity anomalies, on the other hand, demonstrates that SSS anomalies are not in phase with accompanying SST anomalies. After the end of the anomalous Aleutian low forcing, SST anomalies probably dissipate (at least, due to negative feedback in outgoing longwave radiation and latent heat flux) thus resulting in uncompensated surface salinity anomalies (mostly governed by the advection, e.g., Foltz et al., 2004). As a result, these mixed layer salinity and temperature anomalies are not density compensating. Instead, the observed SSS anomalies are maintained by the mixed layer's overall static stability. This implies a certain ΔS threshold on the magnitude of mixed layer salty anomalies that prevents them from vertical overturning. Possibly, a part (compensated) of the original T and S anomaly penetrates in the thermocline when there is anomalous southward Ekman advection and subduction below less dense subtropical gyre water.

Both observations and simulations indicate that changes in the strength of Aleutian Low governing changes in midlatitude westerly winds over the North Pacific are a plausible cause of eastward salinity anomalies via the meridional Ekman advection. While a PDO-like SST pattern develops concurrently with winds and MSLP, an initial salinity anomaly forms in the western Pacific SAF region a year or two after the Aleutian Low change event. The sign of the SSS anomaly is consistent with the direction of anomalous Ekman transport, with salty and fresh SSS anomalies originating in response to anomalously weak and strong westerly winds, respectively. Although the initial SSSA pattern is local and limited to the western Pacific KOE region, it is only the beginning of its evolution. Over the next ten years, it crosses the Pacific, approaching the US west coast in about 5 years, and continues southward along the eastern ocean boundary. The advective behavior of SAF salinity anomalies implies a multi-year time lag between their central North Pacific crossing and US west coast appearance, which provides a potential mechanism for their predictability. The characteristic period of these oscillations, which is 5 years, is expected to define the temporal scale of predictability.

Because all basins have frontal interfaces with high gradients separating warm and salty subtropical gyres from cool and fresh subpolar gyres, one may speculate that similar eastward salinity propagation may be expected there, including the North Atlantic Current, e.g., (Holliday et al., 2020) and South Indian Ocean (Sun et al., 2019), where favorable conditions for salinity anomaly propagation out of western boundaries exist. Eastward salinity anomalies caused by Amazon plume variability have recently been described in the Atlantic North Equatorial Countercurrent (Grodsky et al., 2022).

This descriptive study leaves unanswered several important questions pertaining to these eastward-traveling salinity anomalies. Given the relatively long zonal scale of wind variability, it is partially unclear how and why such anomalies are generated primarily in the west but not along the entire SAF. As they approach the US west coast, the eastward salinity anomalies enter the California/Alaska Current bifurcation zone and could be expected to take either a southward or a northward pathway in the California and Alaska Current, respectively. However, our time-limited observations indicate that they primarily follow the southern pathway. On longer, multidecadal periods Pozo and Di Lorenzo (2015) show that subsurface temperature anomalies generated along the North Pacific Current significantly contribute to decadal changes of SST in

the Gulf of Alaska. Finally, what role, if any, does salinity advection play in heatwave blobs along the US west coast via its effect on static haline stability (Zhi et al., 2019)?

Acknowledgments. This research was supported by the NASA Ocean Sea Surface Salinity Team.

References

Carton, J.A., Grodsky, S.A., Liu, H., 2008. Variability of the oceanic mixed layer, 1960-2004. J. Clim. 21, 1029–1047. doi:10.1175/2007JCLI1798.1

Cummins, P.F., Lagerloef, G.S.E., Mitchum, G., 2005. A regional index of northeast Pacific variability based on satellite altimeter data. Geophys. Res. Lett. 32. doi:10.1029/2005GL023642

Di Lorenzo, E., Schneider, N., Cobb, K.M., Franks, P.J.S., Chhak, K., Miller, A.J., McWilliams, J.C., Bograd, S.J., Arango, H., Curchitser, E., Powell, T.M., Rivière, P., 2008. North Pacific Gyre Oscillation links ocean climate and ecosystem change. Geophys. Res. Lett. 35, L08607. doi:10.1029/2007GL032838

Dunne, J.P., Horowitz, L.W., Adcroft, A.J., Ginoux, P., Held, I.M., John, J.G., Krasting, J.P., Malyshev, S., Naik, V., Paulot, F., Shevliakova, E., Stock, C.A., Zadeh, N., Balaji, V., Blanton, C., Dunne, K.A., Dupuis, C., Durachta, J., Dussin, R., Gauthier, P.P.G., Griffies, S.M., Guo, H., Hallberg, R.W., Harrison, M., He, J., Hurlin, W., McHugh, C., Menzel, R., Milly, P.C.D., Nikonov, S., Paynter, D.J., Ploshay, J., Radhakrishnan, A., Rand, K., Reichl, B.G., Robinson, T., Schwarzkopf, D.M., Sentman, L.T., Underwood, S., Vahlenkamp, H., Winton, M., Wittenberg, A.T., Wyman, B., Zeng, Y., Zhao, M., 2020. The GFDL Earth System Model Version 4.1 (GFDL-ESM 4.1): Overall Coupled Model Description and Simulation Characteristics. J. Adv. Model. Earth Syst. 12, e2019MS002015. doi:10.1029/2019MS002015

Foltz, G.R., Grodsky, S.A., Carton, J.A., McPhaden, M.J., 2004. Seasonal salt budget of the northwestern tropical Atlantic Ocean along 38°W. J. Geophys. Res. Ocean. 109, C03052. doi:10.1029/2003JC002111

Grodsky, S.A., Carton, J.A., Murtugudde, R., 2001. Anomalous surface currents in the tropical Indian Ocean. Geophys. Res. Lett. 28, 4207–4210. doi:10.1029/2001GL013592

Grodsky, S.A., Reul, N., Bentamy, A., Vandemark, D., 2022. Eastward propagating surface salinity anomalies in the tropical North Atlantic. Remote Sens. Lett. 13, 334–342. doi:10.1080/2150704X.2022.2032452

Hersbach, H., Bell, B., Berrisford, P., Hirahara, S., Horányi, A., Muñoz-Sabater, J., Nicolas, J., Peubey, C., Radu, R., Schepers, D., Simmons, A., Soci, C., Abdalla, S., Abellan, X., Balsamo, G., Bechtold, P., Biavati, G., Bidlot, J., Bonavita, M., Chiara, G., Dahlgren, P., Dee, D., Diamantakis, M., Dragani, R., Flemming, J., Forbes, R., Fuentes, M., Geer, A., Haimberger, L., Healy, S., Hogan, R.J., Hólm, E., Janisková, M., Keeley, S., Laloyaux, P., Lopez, P., Lupu, C., Radnoti, G., Rosnay, P., Rozum, I., Vamborg, F., Villaume, S., Thépaut, J.-N., 2020. The ERA5 global reanalysis. Q. J. R. Meteorol. Soc. 146, 1999–2049. doi:10.1002/qj.3803

Holliday, N.P., Bersch, M., Berx, B., Chafik, L., Cunningham, S., Florindo-López, C., Hátún, H., Johns, W., Josey, S.A., Larsen, K.M.H., Mulet, S., Oltmanns, M., Reverdin, G., Rossby, T., Thierry, V., Valdimarsson, H., Yashayaev, I., 2020. Ocean circulation causes the largest freshening event for 120 years in eastern subpolar North Atlantic. Nat. Commun. doi:10.1038/s41467-020-14474-y

Kao, H.-Y., Lagerloef, G., Lee, T., Melnichenko, O., Meissner, T., Hacker, P., 2018. Assessment of Aquarius Sea Surface Salinity. Remote Sens. 10, 1341. doi:10.3390/rs10091341

Katsura, S., 2018. Properties, formation, and dissipation of the North Pacific Eastern Subtropical Mode Water and its impact on interannual spiciness anomalies. Prog. Oceanogr. 162, 120–131. doi:10.1016/j.pocean.2018.02.023

Killworth, P.D., Chelton, D.B., de Szoeke, R.A., 1997. The Speed of Observed and Theoretical Long Extratropical Planetary Waves. J. Phys. Oceanogr. 27, 1946–1966. doi:10.1175/1520-0485(1997)027<1946:TSOOAT>2.0.CO;2

Kouketsu, S., Osafune, S., Kumamoto, Y., Uchida, H., 2017. Eastward salinity anomaly propagation in the intermediate layer of the North Pacific. J. Geophys. Res. Ocean. 122, 1590–1607. doi:10.1002/2016JC012118

Kouketsu, S., Sasano, D., Osafune, S., Aoyama, M., 2020. Relationships Among Decadal Changes in Nitrate and Salinity in the Eastern and Western North Pacific Ocean After 2000. J. Geophys. Res. Ocean. 125. doi:10.1029/2019JC015016

Liu, H., Grodsky, S.A., Carton, J.A., 2009. Observed subseasonal variability of oceanic barrier and compensated layers. J. Clim. 22, 6104–6119. doi:10.1175/2009JCLI2974.1

Mantua, N.J., Hare, S.R., 2002. The Pacific Decadal Oscillation. J. Oceanogr. 58, 35–44. doi:10.1023/A:1015820616384

Meissner, T., Wentz, F.J., Manaster, A., Lindsley, R., 2019. Remote Sensing Systems SMAP Ocean Surface Salinities [Level 2C, Level 3 Running 8-day, Level 3 Monthly], Version 4.0 validated release. [WWW Document]. doi:0.5067/SMP40-3SMCS

Melnichenko, O., Hacker, P., Maximenko, N., Lagerloef, G., Potemra, J., 2016. Optimum interpolation analysis of Aquarius sea surface salinity. J. Geophys. Res. Ocean. 121, 602–616. doi:10.1002/2015JC011343

Nakamura, H., 2003. Decadal changes in the North Pacific oceanic frontal zones as revealed in ship and satellite observations. J. Geophys. Res. 108, 3078. doi:10.1029/1999JC000085

Newman, M., Alexander, M.A., Ault, T.R., Cobb, K.M., Deser, C., Di Lorenzo, E., Mantua, N.J., Miller, A.J., Minobe, S., Nakamura, H., Schneider, N., Vimont, D.J., Phillips, A.S., Scott, J.D., Smith, C.A., 2016. The Pacific Decadal Oscillation, Revisited. J. Clim. 29, 4399–4427. doi:10.1175/JCLI-D-15-0508.1

Osafune, S., Kouketsu, S., Masuda, S., Sugiura, N., 2020. Dynamical Ocean Response Controlling the Eastward Movement of a Heat Content Anomaly Caused by the 18.6-Year Modulation of Localized Tidally Induced Mixing. J. Geophys. Res. Ocean. 125, e2019JC015513. doi:10.1029/2019JC015513

Overland, J.E., Salo, S., Adams, J.M., 1999. Salinity signature of the Pacific Decadal Oscillation. Geophys. Res. Lett. 26, 1337–1340. doi:10.1029/1999GL900241

Pozo Buil, M., Di Lorenzo, E., 2015. Decadal changes in Gulf of Alaska upwelling source waters. Geophys. Res. Lett. 42, 1488–1495. doi:10.1002/2015GL063191

Ren, A.S., Rudnick, D.L., 2021. Temperature and salinity extremes from 2014-2019 in the California Current System and its source waters. Commun. Earth Environ. 2, 62. doi:10.1038/s43247-021-00131-9

Reul, N., Grodsky, S.A., Arias, M., Boutin, J., Catany, R., Chapron, B., D'Amico, F., Dinnat, E., Donlon, C., Fore, A., Fournier, S., Guimbard, S., Hasson, A., Kolodziejczyk, N., Lagerloef, G., Lee, T., Le Vine, D.M., Lindstrom, E., Maes, C., Mecklenburg, S., Meissner, T., Olmedo, E., Sabia, R., Tenerelli, J., Thouvenin-Masson, C., Turiel, A., Vergely, J.L., Vinogradova, N., Wentz, F., Yueh, S., 2020. Sea surface salinity estimates from spaceborne L-band radiometers: An overview of the first decade of observation (2010–2019). Remote Sens. Environ. 242, 111769. doi:10.1016/j.rse.2020.111769

Reynolds, R.W., Smith, T.M., Liu, C., Chelton, D.B., Casey, K.S., Schlax, M.G., 2007. Daily High-Resolution-Blended Analyses for Sea Surface Temperature. J. Clim. 20, 5473–5496. doi:10.1175/2007JCLI1824.1

Roemmich, D., Gilson, J., 2009. The 2004–2008 mean and annual cycle of temperature, salinity, and steric height in the global ocean from the Argo Program. Prog. Oceanogr. 82, 81–100. doi:10.1016/j.pocean.2009.03.004

Sasaki, Y.N., Schneider, N., Maximenko, N., Lebedev, K., 2010. Observational evidence for propagation of decadal spiciness anomalies in the North Pacific. Geophys. Res. Lett. 37, n/a-n/a. doi:10.1029/2010GL042716

Sun, Q., Du, Y., Zhang, Y., Feng, M., Chowdary, J.S., Chi, J., Qiu, S., Yu, W., 2019. Evolution of Sea Surface Salinity Anomalies in the Southwestern Tropical Indian Ocean During 2010–2011 Influenced by a Negative IOD Event. J. Geophys. Res. Ocean. 124, 3428–3445. doi:10.1029/2018JC014580

Taguchi, B., Schneider, N., 2014. Origin of Decadal-Scale, Eastward-Propagating Heat Content Anomalies in the North Pacific*. J. Clim. 27, 7568–7586. doi:10.1175/JCLI-D-13-00102.1

Vazquez-Cuervo, J., Gomez-Valdes, J., 2018. SMAP and CalCOFI Observe Freshening during the 2014–2016 Northeast Pacific Warm Anomaly. Remote Sens. 10, 1716. doi:10.3390/rs10111716

Wang, T., Suga, T., Kouketsu, S., 2022. Spiciness anomalies in the upper North Pacific based on Argo observations. Front. Mar. Sci. 9. doi:10.3389/fmars.2022.1006042

Yuan, X., Talley, L.D., 1996. The subarctic frontal zone in the North Pacific: Characteristics of frontal structure from climatological data and synoptic surveys. J. Geophys. Res. Ocean. 101, 16491–16508. doi:10.1029/96JC01249

Zhang, Y., Wallace, J.M., Battisti, D.S., 1997. ENSO-like Interdecadal Variability: 1900–93. J. Clim. 10, 1004–1020. doi:10.1175/1520-0442(1997)010<1004:ELIV>2.0.CO;2

Declaration of interests

☒The authors declare that they have no known competing financial interests or personal relationships that could have appeared to influence the work reported in this paper.

☐The authors declare the following financial interests/personal relationships which may be considered as potential competing interests:

Satellite salinity shows that SSS variability in the North Pacific subarctic front is noticeably different from SST variability.

In contrast to the SST, the SSS (~0.5 psu) propagates eastward crossing the Pacific over five years.

SSS anomalies continue south along the California coast, remaining detectable until the southern tip of the California peninsula.